Article

Cell Reports

Structural and Dynamic Basis for Low-Affinity, High-Selectivity Binding of L-Glutamine by the Glutamine Riboswitch

Graphical Abstract

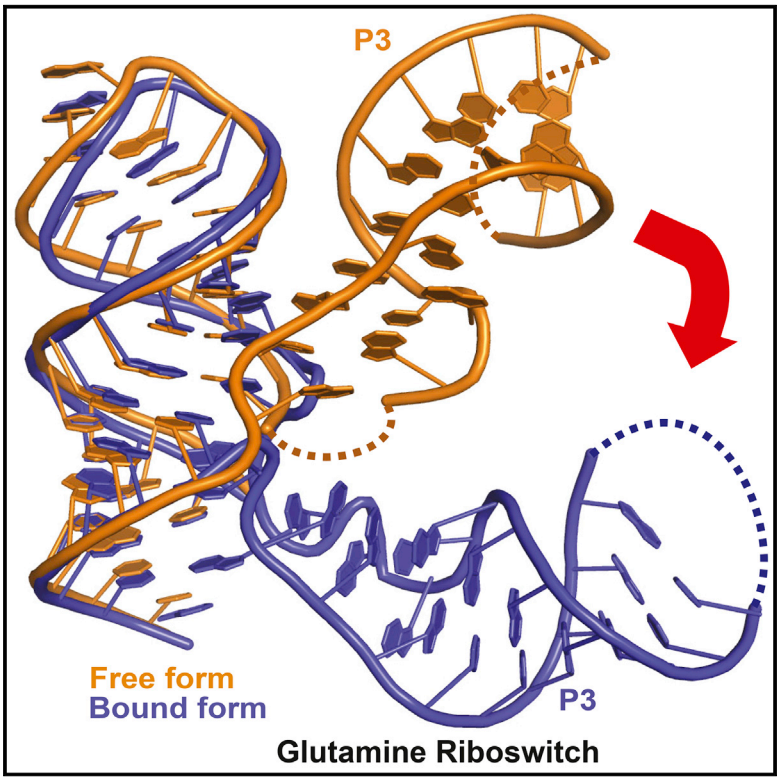

Highlights

- Structural analysis of a glutamine riboswitch in free and L-glutamine-bound states
- L-glutamine complex formation induces a tuning fork to L-shaped conformational transition
- A long-range linchpin Watson-Crick G-C pair-capping interaction drives complex formation
- The conformational change underlies low-affinity, high-selectivity L-glutamine binding

Authors

Aiming Ren, Yi Xue, Alla Peselis, Alexander Serganov, Hashim M. Al-Hashimi, Dinshaw J. Patel

Correspondence

hashim.al.hashimi@duke.edu (H.M.A.-H.), pateld@mskcc.org (D.J.P.)

In Brief

Ren et al. report on the structural and dynamic basis of low-affinity, high-selectivity binding of L-glutamine by the glutamine riboswitch. Molecular recognition of the bound L-glutamine in an open pocket is driven by a long-range linchpin G-C pairing capping interaction, resulting in a tuning fork to L-shaped conformational transition.

Ren et al., 2015, Cell Reports *13*, 1800–1813
December 1, 2015
http://dx.doi.org/10.1016/j.celrep.2015.10.062

CellPress

OPEN ACCESS
CellPress

Cell Reports
Article

Structural and Dynamic Basis for Low-Affinity, High-Selectivity Binding of L-Glutamine by the Glutamine Riboswitch

Aiming Ren,[1,4] Yi Xue,[2,4] Alla Peselis,[3] Alexander Serganov,[3] Hashim M. Al-Hashimi,[2,*] and Dinshaw J. Patel[1,*]
[1]Structural Biology Program, Memorial Sloan-Kettering Cancer Center, New York, NY 10065, USA
[2]Department of Biochemistry and Chemistry, Duke University Medical Center, Durham, NC 27710, USA
[3]Department of Biochemistry and Molecular Pharmacology, New York University School of Medicine, New York, NY 10016, USA
[4]Co-first author
*Correspondence: hashim.al.hashimi@duke.edu (H.M.A.-H.), pateld@mskcc.org (D.J.P.)
http://dx.doi.org/10.1016/j.celrep.2015.10.062

SUMMARY

Naturally occurring L-glutamine riboswitches occur in cyanobacteria and marine metagenomes, where they reside upstream of genes involved in nitrogen metabolism. By combining X-ray, NMR, and MD, we characterized an L-glutamine-dependent conformational transition in the *Synechococcus elongatus* glutamine riboswitch from tuning fork to L-shaped alignment of stem segments. This transition generates an open ligand-binding pocket with L-glutamine selectivity enforced by Mg^{2+}-mediated intermolecular interactions. The transition also stabilizes the P1 helix through a long-range "linchpin" Watson-Crick G-C pair-capping interaction, while melting a short helix below P1 potentially capable of modulating downstream readout. NMR data establish that the ligand-free glutamine riboswitch in Mg^{2+} solution exists in a slow equilibrium between flexible tuning fork and a minor conformation, similar, but not identical, to the L-shaped bound conformation. We propose that an open ligand-binding pocket combined with a high conformational penalty for forming the ligand-bound state provide mechanisms for reducing binding affinity while retaining high selectivity.

INTRODUCTION

Amino acids are critical for protein biosynthesis and many other cellular processes. To keep the adequate intracellular levels of amino acids, bacteria employ different regulatory strategies that involve feedback regulation by amino-acid-sensing proteins and non-coding RNAs. Though much knowledge has been accumulated on the role of proteins in controlling amino acid biosynthesis and transport, less is known about how RNAs recognize amino acids and regulate their concentrations. Many bacteria indirectly control amino acid levels through T-box RNA elements that discriminate between aminoacylated and non-aminoacylated tRNAs (Green et al., 2010) and through riboswitches that respond to cofactors containing amino acid moieties (Serganov and Nudler, 2013). In addition to indirect control, three abundant riboswitches directly sense L-glycine (Mandal et al., 2004), L-lysine (Grundy et al., 2003; Sudarsan et al., 2003) and L-glutamine (Ames and Breaker, 2011) and regulate expression of associated genes. Whereas structural studies have provided insights into the specific recognition of lysine and glycine by riboswitches, how "*glnA*" and related "downstream peptide" riboswitch motifs select their cognate ligand L-glutamine and modulate gene expression remains unclear.

Specific recognition of cellular metabolites is a prerequisite for modulation of gene control by riboswitches (Mironov et al., 2002; Nahvi et al., 2002; Winkler et al., 2002). The underlying principle governing riboswitch function dictates that metabolite binding triggers a structural rearrangement in the metabolite-sensing domain of the riboswitch that modulates the formation of the "regulatory" P1 helix, thereby changing the folding of the downstream expression platform responsible for gene expression control (Breaker, 2011; Serganov and Nudler, 2013).

Structural and biochemical studies showed that ligand binding in most cases stabilizes the P1 helix by engaging its "upper" portion in the ligand-binding pocket and through formation of stabilizing inter-helical stacking interactions mediated by either remote ligand binding or by direct contacts with the bound ligand (Serganov and Patel, 2012).

Ligand-dependent conformational changes in the sensing domain form the basis for modulating the structure of the expression platform and ultimately gene regulation by riboswitches. To visualize ligand-dependent conformational rearrangements, several studies reported high-resolution X-ray structures for some metabolite-sensing domains in both the absence and presence of ligand. These structures revealed only minor differences in local structure in and around the binding pocket (Butler et al., 2011; Garst et al., 2008; Huang et al., 2010; Serganov et al., 2008; Stoddard et al., 2010). For example, the ligand-free structures of the lysine and glycine riboswitches are remarkably similar to their ligand-bound structures while lacking the ligand and an associated cation in a preformed ligand-binding pocket (Garst et al., 2008; Huang et al., 2010; Serganov et al., 2008). The sensing domains of SAM-I (Montange and Batey, 2006; Stoddard

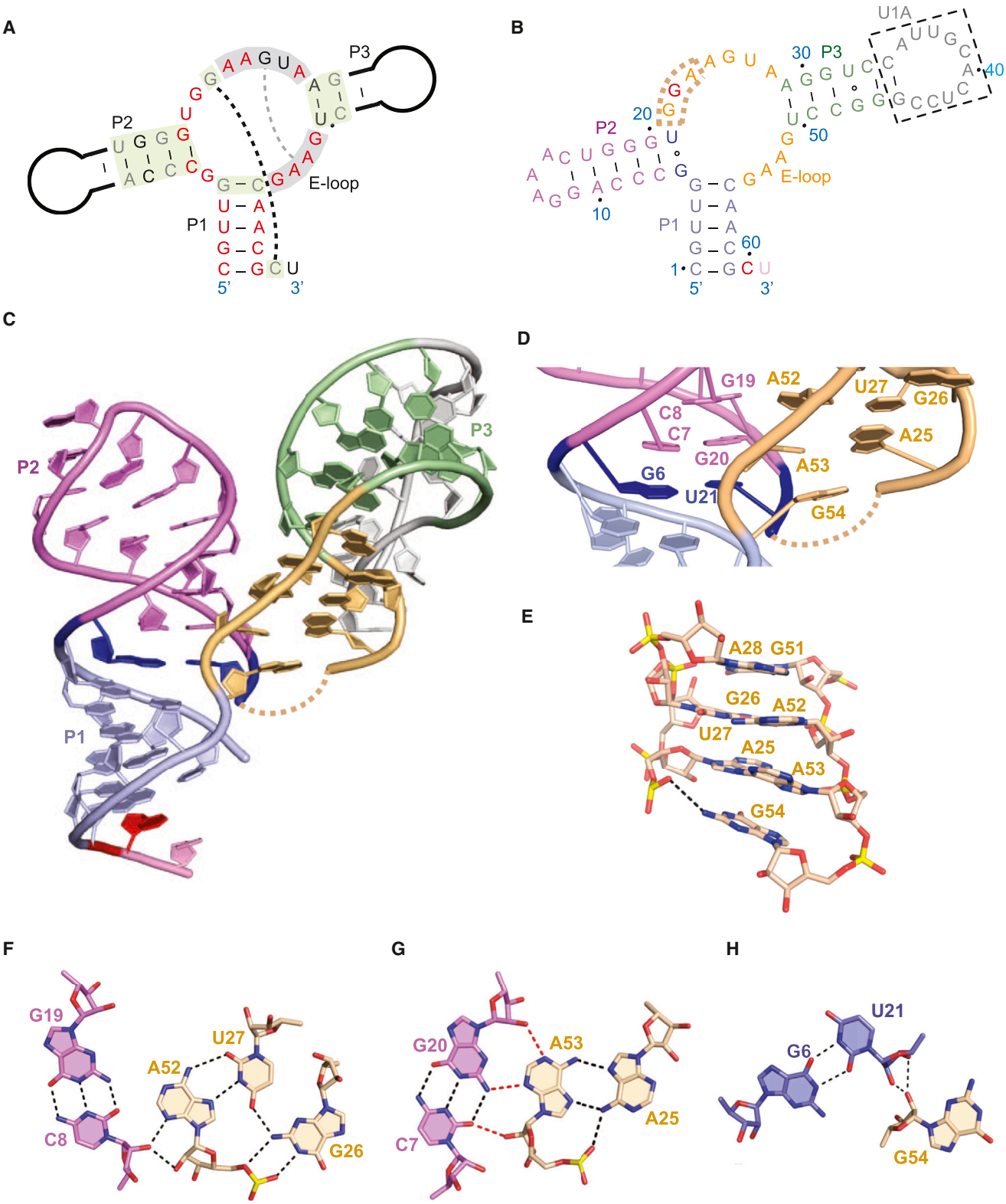

Figure 1. Crystal Structure of the *S. elongatus* Glutamine Riboswitch in the Free State

(A) Consensus sequence and secondary structure models of the glutamine riboswitch.

(B) The sensing domain of the GU glutamine riboswitch construct used for crystallization. G23 and C60, which form a long-range "linchpin" Watson-Crick base pair in the L-glutamine-bound state, are in red.

(legend continued on next page)

et al., 2010) and preQ$_1$-I (Jenkins et al., 2011; Klein et al., 2009) riboswitches also adopt similar overall structures in free and ligand-bound states with a nucleotide base occupying the ligand-binding pocket in the ligand-free structure. Yet studies employing in-line chemical probing, NMR, small-angle X-ray scattering (SAXS), single-molecule Förster resonance energy transfer (FRET), and computational modeling strongly suggest that, in the absence of ligand, the sensing domain adopts a flexible conformation and that, in most cases, ligand binding is accompanied by stabilization of the P1 helix (Chen et al., 2012; Serganov et al., 2004; Stoddard et al., 2010; Zhang et al., 2014). To date, high-resolution structures for sensing domains that differ significantly between the ligand-free and bound states, as would be expected for a functional regulatory switch, have not been reported, thereby limiting our basic understanding regarding the nature and range of the ligand-free ensemble.

Ligand-dependent conformational changes could in principle play other roles in riboswitches. Riboswitches need to selectively recognize metabolites, as well as tune their response to what are often high cellular metabolite concentrations. Thus, whereas high-affinity binding is typically required to achieve high selectivity, this can result in premature genetic switching at concentrations much lower than the physiological metabolite concentration. There is evidence that some transcriptional riboswitches employ kinetic strategies to increase the metabolite concentration needed for switching above the dissociation constant (K_d) for ligand binding (Wickiser et al., 2005). Considering that sensing domains of riboswitches bind their ligands with affinities that span more than seven orders of magnitude (K_d = 10 pM–600 μM; Breaker, 2011; Serganov and Nudler, 2013), there is also evidence that sensing domains can directly tune their binding affinities. How riboswitches tune down their binding affinity while maintaining high selectivity is not as yet fully understood. By imparting variable energetic penalties toward forming the competent ligand-bound state, ligand-dependent conformational changes in the sensing domain could in principle play roles in tuning down ligand binding affinity.

The recently discovered L-glutamine-binding *glnA* motif (Figure 1A) provides a striking example of a metabolite-sensing RNA capable of low-affinity, high-selectivity ligand binding. These RNA sequences are found exclusively in cyanobacteria and marine metagenomic sequences, where they reside upstream of genes involved in nitrogen metabolism. These riboswitches bind to their cognate ligand, L-glutamine, with very weak dissociation constants (K_d) in the high μM range (Ames and Breaker, 2011), in contrast to other riboswitches that bind their ligands with tighter affinities in the low μM to nM range (Serganov and Nudler, 2013). Yet the L-glutamine-sensing motifs strongly discriminate against related ligands including L-glutamate (Ames and Breaker, 2011). Low-affinity, high-selectivity binding may be important for an RNA-based switch given the exceptionally high intracellular concentration of L-glutamine reported for bacteria (Bennett et al., 2009).

Here, we report on structural and dynamics studies of the L-glutamine-sensing domain of the *glnA* riboswitch from *Synechococcus elongatus* (henceforth labeled glutamine riboswitch for simplicity) in the ligand-free and L-glutamine-bound states. These studies reveal a large ligand-dependent structural transition from a tuning-fork-like conformation in the ligand-free form to an L-shaped architecture in the ligand-bound form. The ligand-bound structure helps explain the selectivity of the glutamine riboswitch for L-glutamine and the basis for discrimination against related molecules. NMR studies and molecular dynamics (MD) simulations show that, in the absence of ligand but in the presence of Mg^{2+}, the glutamine riboswitch exists in a slow dynamic equilibrium between flexible tuning fork and a minor species that is similar, but not identical, to the L-shaped bound conformation. We propose that high selectivity is achieved despite low-affinity ligand binding in part by imposing an energetic penalty to forming a conformation needed for specific ligand recognition. This energetic penalty most likely arises due to the requirement to form a precise long-range "linchpin" G-C base pair, which is a key tertiary element of the ligand-bound structure. In addition, the formation of an open ligand-binding pocket in the ligand-bound form is also expected to contribute to the reduced binding affinity.

RESULTS

Construct Design for X-ray Structural Studies of the Glutamine Riboswitch

Our X-ray structural studies have been undertaken on two constructs of the sensing domain of the glutamine riboswitch, one of which contains G6 positioned opposite U21 (GU glutamine riboswitch; Figure 1B) and another containing A6 opposite C21 (AC glutamine riboswitch). Both GU and AC combinations at these positions have been observed on phylogenetic analysis of the sequences of the sensing domains of the glutamine riboswitch. To facilitate crystallization, the hairpin loops L2 and L3, that are dispensable for L-glutamine binding, were replaced by a stable GAAA tetra-loop and a U1A-protein-binding loop (Oubridge et al., 1995), respectively, resulting in a 61-nt sensing domain construct of the GU glutamine riboswitch (Figure 1B).

Isothermal titration calorimetry (ITC) experiments showed that these alterations do not affect the ligand-binding properties of the RNA. The GU glutamine riboswitch binds to L-glutamine in the absence and presence of U1A with similar K_d values of 117 μM and 154 μM, respectively (Figure S1A; Table S1), which can be compared with the binding affinity of 575 μM determined from in-line probing experiments (Ames and Breaker, 2011).

(C) The tuning-fork-like riboswitch architecture of the GU glutamine riboswitch shown in a ribbon representation in the free state. The bound U1A protein is not shown and can be seen in a surface representation in Figures S2A and S2B.
(D) An expanded view of (C) centered on the three-helical junction. The G22-G23-A24 segment that is disordered in the free state is shown by a dashed box in (B) and by dashed lines in (C) and (D).
(E) The base-paired E-loop fold capped by a stacked G54 base in the free state.
(F–H) Pairing alignments stabilizing the junctional architecture in the free state.
See also Figure S2.

Similar binding affinities are also observed for the binding of the AC glutamine riboswitch to L-glutamine both in the absence and presence of U1A (Figure S1B; Table S1).

Crystal Structure of the GU Glutamine Riboswitch in the Ligand-Free State

Crystallization trials of the GU glutamine riboswitch undertaken with U1A in the absence of L-glutamine but presence of Mg^{2+} yielded crystals that diffracted to 3.1 Å resolution (Table S2; Supplemental Information). The resulting crystal structure revealed a three-way junctional fold (Figures 1C, 1D, S2A, and S2B) that conforms to the consensus secondary structure of the *glnA* motif from phylogenetic analysis (Ames and Breaker, 2011). The fold is reminiscent of a tuning-fork-like architecture, with stem P1 forming the handle, whereas stem P2 (collinear with stem P1) and stem P3 form parallel-aligned prongs. Such an alignment is facilitated by the junctional loop that partially zippers up through formation of a helical E-loop scaffold capped by stacked G54 (Figures 1E and S2D–S2F; Correll et al., 1997) and extends stem P3, leaving a disordered G22-G23-A24 segment (Figures 1C and 1D).

The helical E-loop motif maintains the juxtaposition of stems P2 and P3 through tertiary A-minor interactions and a ribose zipper involving three consecutive base pairs spanning the P1-P2 junction, resulting in formation of a five-base platform (Figure 1F), a maximally paired tetrad (Figure 1G), and a three-base platform (Figure 1H).

Crystal Structure of the AC Glutamine Riboswitch in the L-Glutamine Bound State

Though attempts at crystallization of the GU glutamine riboswitch in the presence of L-glutamine were unsuccessful, we did succeed in generating 2.3 Å crystals of AC glutamine riboswitch in the L-glutamine bound state (Table S2). For this structure of the complex, there are two bound L-glutamine riboswitch molecules in the asymmetric unit, which adopt very similar structures with a RMSD value of 0.80 Å. In stark contrast to the ligand-free structure, the AC glutamine riboswitch in the L-glutamine-bound form adopts an L-shaped-like conformation (Figures 2A, 2B, and S3A). As in the free form of the RNA, P1 collinearly stacks on P2. However, P3 together with collinearly stacked E-loop helix capped by stacked A24 (Figure 2C) adopts a near perpendicular conformation relative to P2. This large change in the orientation of P3 relative to P2 and P1 brings into proximity several residues involved in long-range interactions, including a critical linchpin Watson-Crick G23-C60 pair interaction (see below) lining the ligand-binding pocket (Figure 2B).

The L-glutamine binds to the glutamine riboswitch at the base of P1, in the proximity of the L-shaped junction (Figure 2B). The lower stem of P1 forms a higher-order architecture that connects P1 with both segments of the internal bulge. This structure contains major groove-aligned G54•(A56-U4) (Figure 2D) and G22•(G2-C58) (Figure 2E) triples and a *trans* Watson-Crick-aligned A•C non-canonical pair (Figure 2F), with this topology stabilized by the newly formed long-range linchpin Watson-Crick G23-C60 pair that stacks under the terminal C1-G59 pair, effectively capping and stabilizing the P1 helix (Figure 2G). Thus, G22 and G23, which are disordered in the free RNA, form key long-range interactions in the ligand-bound state. Notably, the linchpin G23-C60 pairing was postulated from in-line probing and comparative sequence analysis (Ames and Breaker, 2011).

The Binding Pocket for L-Glutamine in the Glutamine Riboswitch

The bound L-glutamine is positioned in a pocket between the major groove edge of the P1-P2 stem and the backbone (phosphate of A53-G54 step; labeled by an arrow) of the E-loop and is bound to an Mg^{2+} cation (Figure 2G). Carboxylate oxygens of the ligand form direct (inner sphere) and water-mediated (outer sphere) coordination bonds with an octahedrally coordinated Mg^{2+} cation (Figures 2G and 2H). Mg^{2+} cations were validated by observing the anomalous signal in soaks with Mn^{2+} cation, which reveal divalent cation-binding sites (Figures S3B and S3C), but not in soaks with Cs^{+} cation, which reveal monovalent cation-binding sites (Figure S3D).

The Mg^{2+} cation mediates the vast majority of interactions to the major groove triples above the bound ligand and helps to maintain the conformation of the pocket by bridging the RNA strands (Figures 2G and 2H). Consistent with the structure, ITC data show that ligand binding strongly depends on Mg^{2+} cations (Figure S1C). L-glutamine also binds the glutamine riboswitch in the presence of related Mn^{2+} cations, whereas other divalent cations, such as Ca^{2+} and Ba^{2+} do not support efficient L-glutamine binding. These results demonstrate high selectivity of the glutamine riboswitch to Mg^{2+} and Mn^{2+} cations (Figure S1D).

The main chain amine group and side chain carbonyl of the bound L-glutamine make base-specific hydrogen bonds with the major groove of the C1-G59 base pair, whereas the side chain amine hydrogen bonds to the backbone phosphate of G54 (Figure 2I). Strikingly, the carboxamide group of the L-glutamine side chain is sandwiched between G22 and G23 (Figure 2J), such that the G22-G23-A24 segment that is disordered in the ligand-free state (Figure 1C) forms a three-sided box to accommodate this group in the ligand-bound state (Figure 2G).

Consistent with prior studies probing the binding selectivity of the glutamine riboswitch for glutamine analogs using in-line probing (Ames and Breaker, 2011), ITC binding data establish the high selectivity of the glutamine riboswitch studied here, given that it does not bind to D-glutamine, L-glutamate, and L-asparagine (Figure S1E; Table S1), as well as L-glutamine methyl and t-butyl esters (Figure S1F; Table S1). Notably, ITC experiments showed that L-glutamine binding is completely lost on replacing the critical Watson-Crick C1-G59 pair by its G1-C59 counterpart (Figure S1G; Table S1), which, as anticipated, would disrupt the intermolecular hydrogen bond recognition network (Figure 2I).

Unlike most riboswitches, the glutamine riboswitch binds L-glutamine in a relatively open pocket (Figure 2H). Thus, although the structure is capable of discriminating against related ligands, it does so using a strategy that does not entirely envelope the ligand. This could help reduce the binding affinity by increasing the off rates of the ligand.

Limited Sampling of the Ligand-Bound Structure in the Absence of Ligand from Computational Simulations

The X-ray structures suggest a dramatic ligand-dependent change in structural features on complex formation. This raised

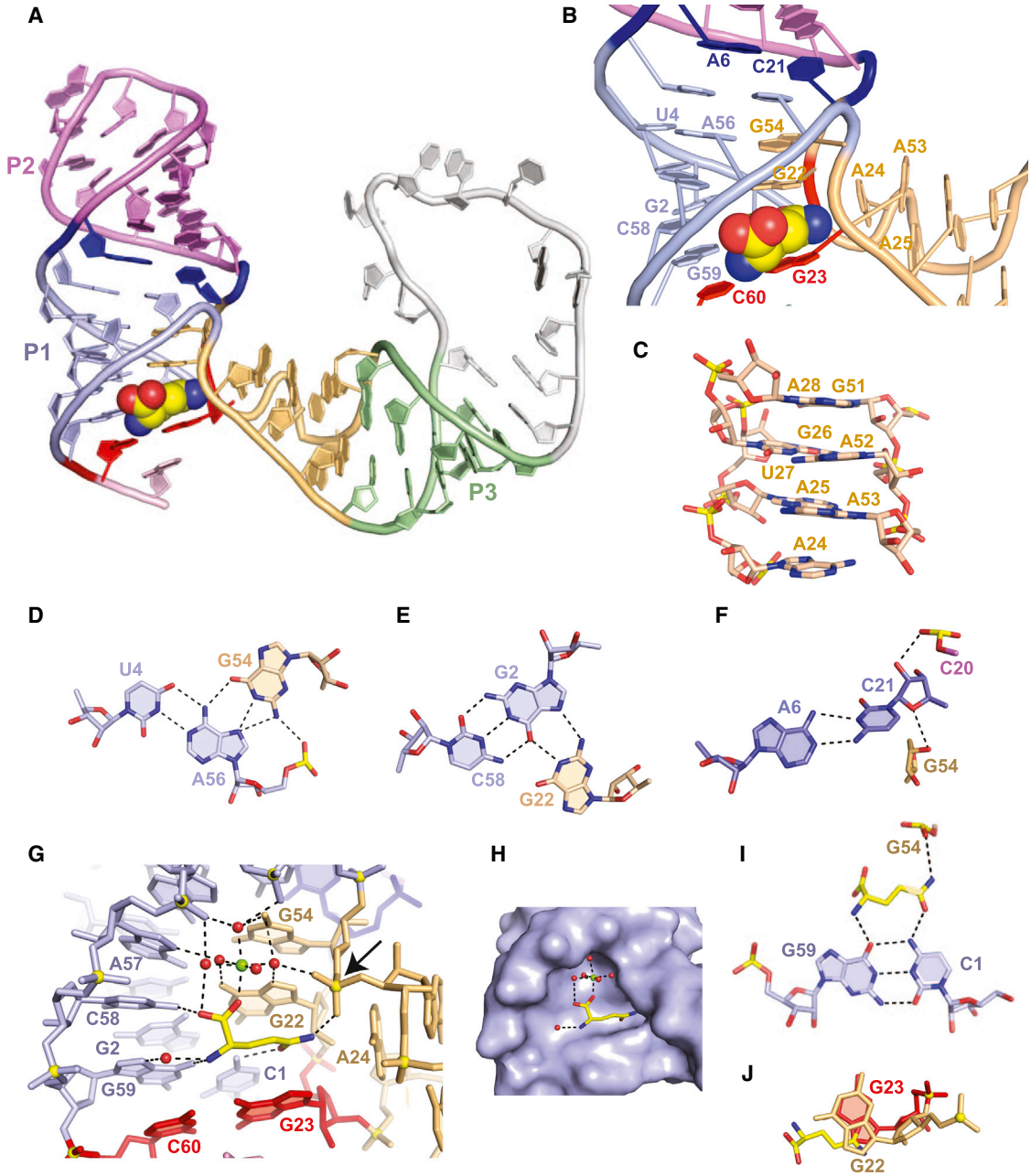

Figure 2. Crystal Structure and Intermolecular Interactions within the Binding Pocket of the Glutamine Riboswitch in the L-Glutamine Bound State

(A) The L-shaped architecture of the AC glutamine riboswitch in a ribbon representation bound to L-glutamine in a space-filling representation. The bound U1A protein is not shown and can be seen in a surface representation in Figure S3A.

(B) An expanded view of (A) centered on the three-helical junction with bound L-glutamine (space-filing representation). The long-range linchpin Watson-Crick G23-C60 pair is shown in red.

(C) The base-paired E-loop fold capped by a stacked A24 base in the bound state.

(D and E) Major groove triples stabilizing the junctional architecture in the bound state.

(F) Formation of a trans Watson-Crick A6•C21 non-canonical pair in the bound state.

(G) Interactions between L-glutamine, RNA, Mg^{2+} cation (green sphere), and water molecules (red spheres) in the structure of the complex. Intermolecular hydrogen bonds and Mg^{2+} coordination bonds are depicted by dashed lines.

(H) The same view as in (G), with the RNA in a surface representation.

(I) Pairing alignments involving the bound L-glutamine in the bound state.

(J) Intercalation of the carboxamide group of the side chain of L-glutamine between G22 and G23 bases in the bound state.

See also Figure S3.

the possibility that lower binding affinity is also achieved in part by imposing an energetic penalty to forming the conformation capable of high binding selectivity. In the simplest model, the apparent binding affinity (K_{app}) is diminished by an amount inversely proportional to the equilibrium constant between the free and bound structures in the absence of ligand (K_{eq}):

$$K_{app} \sim (1/K_{eq}) \times K_d,$$

where K_d is the dissociation constant for binding to the ligand-binding competent conformation.

Therefore, to gain insights into the equilibrium dynamics between free and bound conformations in the absence of ligands, we subjected both the free and ligand-bound glutamine riboswitch X-ray structures to accelerated molecular dynamics (aMD) simulations (Hamelberg et al., 2004) in a water box equilibrated with monovalent Na^+ ions. The aMD allows for broader sampling of conformational space, allowing more-effective comparison of the conformational preferences for the free and ligand-bound states. We focused specifically on dynamic sampling involving the inter-helical Euler angles between P2 and P3 defined in Figure 3A (Bailor et al., 2011), which undergo large changes between the free and bound forms (see Figures 3B and 3C, where ligand-free and bound form X-ray structures are represented by black cross and red cross, respectively). The ligand was removed in silico from the ligand-bound structure prior to the MD simulation of the ligand-bound form to avoid difficulties in modeling critical interactions with Mg^{2+} ions (Auffinger, 2012). This also allowed us to gain insights into the stability of the bound RNA structure in the absence of ligand and to compare its behavior to that of the distinct ligand-free structure.

aMD simulations of the free form structure show large variations in the P2-P3 inter-helical angles (Figure 3B). We observe an energetic minimum at inter-helical angles similar, but not identical, to the ligand-bound state (Figure 3B). Similarly, the long-range linchpin base pair is not observed during the aMD simulations in the free state (Figures 3D and 3E). The bound P2-P3 inter-helical conformation is also minimally sampled in coarse-grained simulations using TOPRNA (Mustoe et al., 2014), in which sampling is only limited by simple topological constraints (Figure S4A). This was the case even after imposing long-range linchpin and zipper pairing (Figure S4B). By analyzing the tertiary contact map derived from TOPRNA simulation, we find a significantly higher energetic penalty for forming a linchpin contact in glutamine riboswitch ($\Delta G = 4.7$ kcal mol^{-1}; see Figure S4C) as compared to tertiary contacts in tRNA computed using the same coarse-grained model ($\Delta G = 1.2$–3.6 kcal mol^{-1}; Mustoe et al., 2014). For comparison, TOPRNA simulation on the c-di-GMP riboswitch (Kulshina et al., 2009), which has a much-higher ligand-binding affinity ($K_d \sim 1$ nM) yields a free energy cost as low as 2.3 kcal mol^{-1} on formation of an analogous long-range base pair similar to the linchpin interaction in glutamine riboswitch (Figure S4D). These data suggest that the ligand-bound L-shaped tertiary structure of the glutamine riboswitch is energetically unfavorable in the absence of ligands. Interestingly, transitions between the free and ligand-bound-like conformations are also accompanied by partial melting of the P1 helix (see RMSD profile in Figure 3B and the middle model shown in Figure 3D), and this could also represent a significant kinetic barrier for inter-conversion between the two states. On the other hand, bound-form aMD simulations do not sample the free P2-P3 inter-helical conformations (Figure 3C). Reduced inter-helical dynamics was observed despite the fact that the ligand was not present during the course of the simulation. Thus, even when taking into account the range of structures available to the ligand-bound state, the free glutamine riboswitch shows limited sampling of the ligand-bound conformation.

NMR Spectra of E-Glutamine Riboswitch in Absence and Presence of Mg^{2+} and Added L-Glutamine

The computational simulations suggest that the ligand-bound conformation is not energetically favorable in the absence of ligand. To further examine this possibility, and gain insights into the ligand-dependent conformational transition under solution conditions, we performed solution NMR experiments on a uniformly ^{13}C,^{15}N-labeled extended-glutamine riboswitch construct (E-glutamine riboswitch), which is identical to that used in the X-ray structures of the free form except for two differences: (1) the apical loops of P2 and P3 were replaced with the wild-type sequence and (2) the P1 helix was extended in accordance with the wild-type sequence and capped with a 5′-guanine to facilitate in vitro transcription (Figure 4A). Compared to other techniques used to study structure and dynamics, NMR spectroscopy is uniquely capable of assessing transitions toward species such as ligand-bound states that may be only weakly populated in solution (Bothe et al., 2011). We collected NMR spectra for uniformly ^{13}C,^{15}N-labeled E-glutamine riboswitch (0.9 mM) under three conditions: (1) absence of both Mg^{2+} and L-glutamine (Figure 4B), (2) presence of 5 mM Mg^{2+} (Figure 4C), and (3) presence of both 5 mM Mg^{2+} and 6 mM L-glutamine (Figure 4D). Resonances were assigned using standard NOESY experiments (see Experimental Procedures and Figure S5).

The imino spectra and NOE distance-based connectivities suggest a common RNA secondary structure across all three conditions (no Mg^{2+}, added Mg^{2+}, and added Mg^{2+} and L-glutamine) that is similar to that observed in the X-ray structures of free and ligand-bound glutamine riboswitch. Nevertheless, comparison of 2D NH and CH spectra reveal marked differences that are consistent with a ligand-induced RNA conformational transition (Figures 4B–4D, S5D, and S5E). The imino resonances that undergo ligand-dependent perturbations (G2, U3, U4, and G59) belong to residues in and around the binding pocket including the linchpin pair (Figures 2B and 2G) and three-base platforms (Figures 2D and 2E). These residues are expected to undergo changes in local environment upon ligand binding (Figures 4B–4D and S5D). One resonance (labeled with "G$^{?}$") that appears on L-glutamine binding can be assigned to a guanine by use of G-selective and U-selective ^{13}C,^{15}N-labeled samples (data not shown) and has an unusually downfield-shifted ^{15}N chemical shift of $\sim$153 ppm, which is unprecedented for imino ^{15}N chemical shifts. This resonance belongs either to G23, which is involved in the linchpin pair, or a residue involved in the three-base platform such as G22 or G54. Analysis of the imino resonance

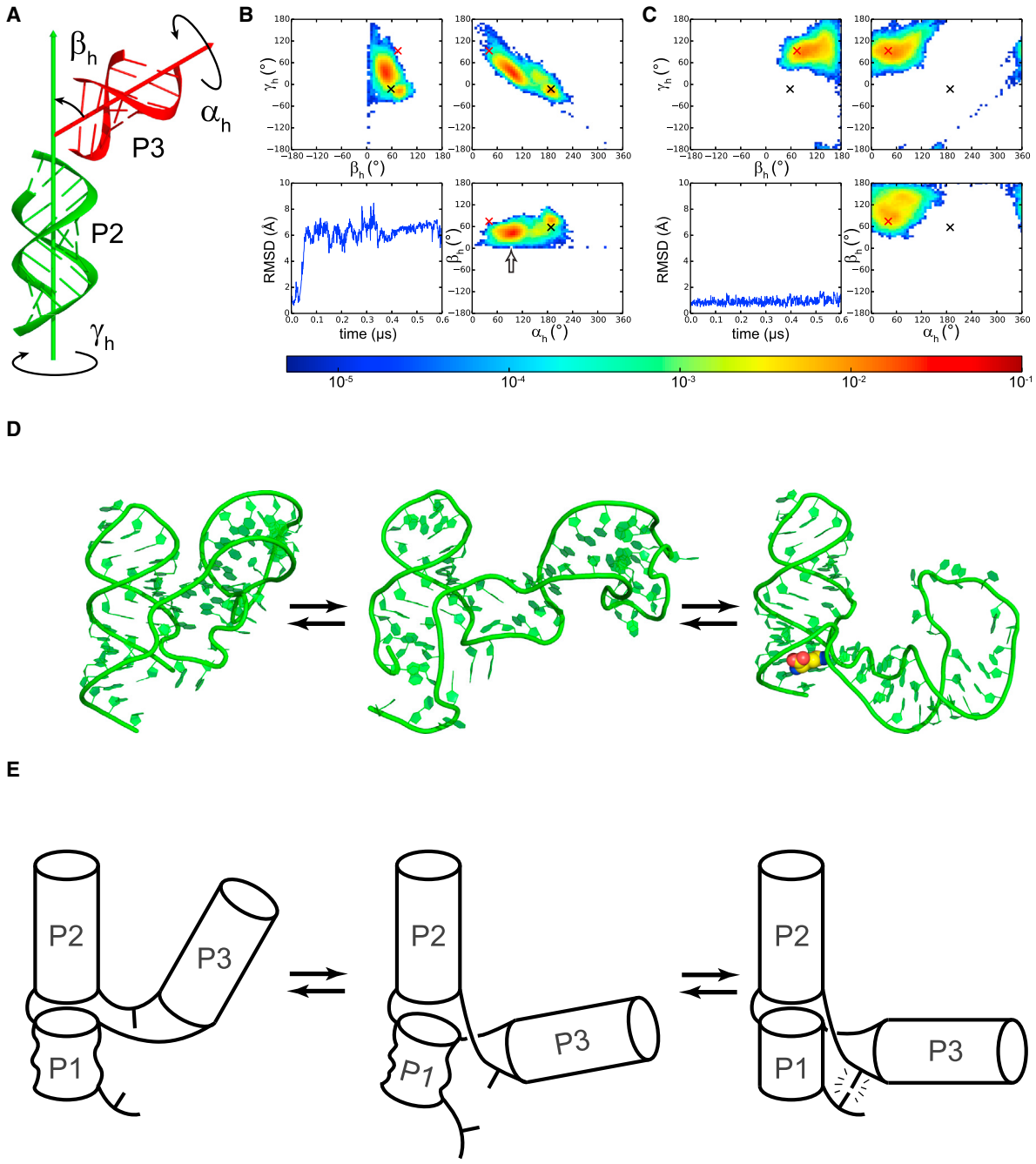

Figure 3. P2-P3 Inter-helical Angle Distributions of Glutamine Riboswitch Derived from aMD Simulations

(A) Definition of the three inter-helical angles describing the orientation of two helices.

(B and C) Inter-helical angle population distributions between P2 and P3 helices obtained from ligand-free-form (B) and bound-form (C) aMD simulations. P2 helix serves as the reference helix. The lower-left panel shows the time course of the root-mean-square deviation (RMSD) of P1 helix relative to an idealized A-form helix when superimposing backbone and sugar atoms. The black and red crosses indicate the ligand-free- and bound-form X-ray structures, respectively. The color bar shows the scale of population.

(D) The proposed conformation transition pathway. The structures on the left and on the right are the ligand-free and bound X-ray structures, respectively. The structure in the middle is a representative conformer, which adopts the bound-form-like inter-helical angles as indicated by the arrow in (B).

(E) Cartoon representation of the transition pathway shown in (D), highlighting the tertiary linchpin and changes in inter-helical conformation.

See also Figure S4.

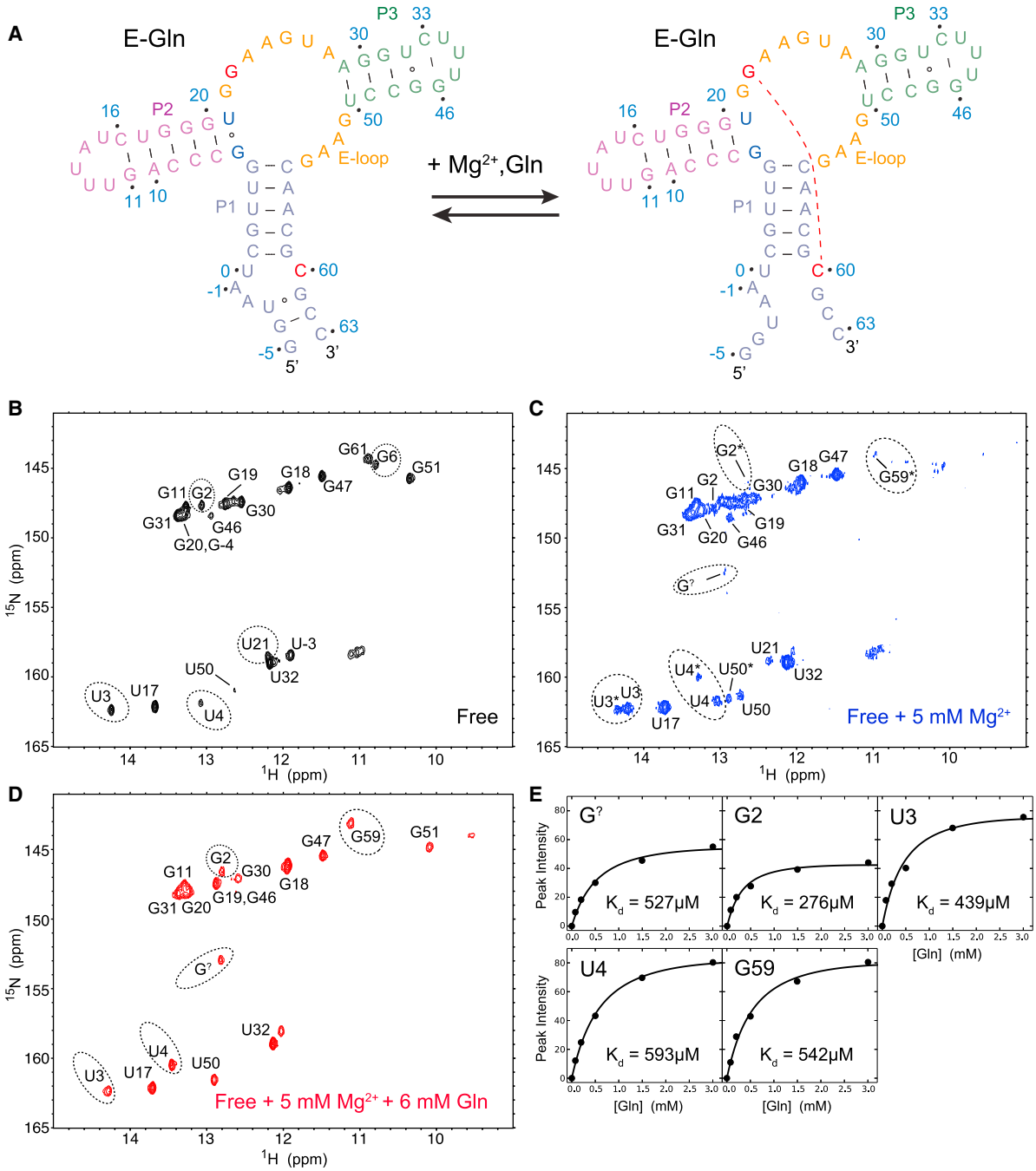

Figure 4. NMR Chemical Shift Mapping of Mg^{2+} and Ligand Binding to the E-Glutamine Riboswitch

(A) Secondary structure of free-form E-glutamine riboswitch (left) in equilibrium with bound-form conformation (right) that is favored by Mg^{2+} and L-glutamine ligand.

(B–D) 2D NH HSQC imino spectra of E-glutamine riboswitch in the absence of Mg^{2+} and L-glutamine (B) in the presence of 5 mM Mg^{2+} (C) and in the presence of 5 mM Mg^{2+} and 6 mM L-glutamine (D). All spectra were recorded at 10°C.

(E) L-glutamine binding curves as monitored by measuring NMR peak intensities for five imino resonances that appear upon incremental addition of L-glutamine. The measurements were conducted at 25°C.

See also Figure S5.

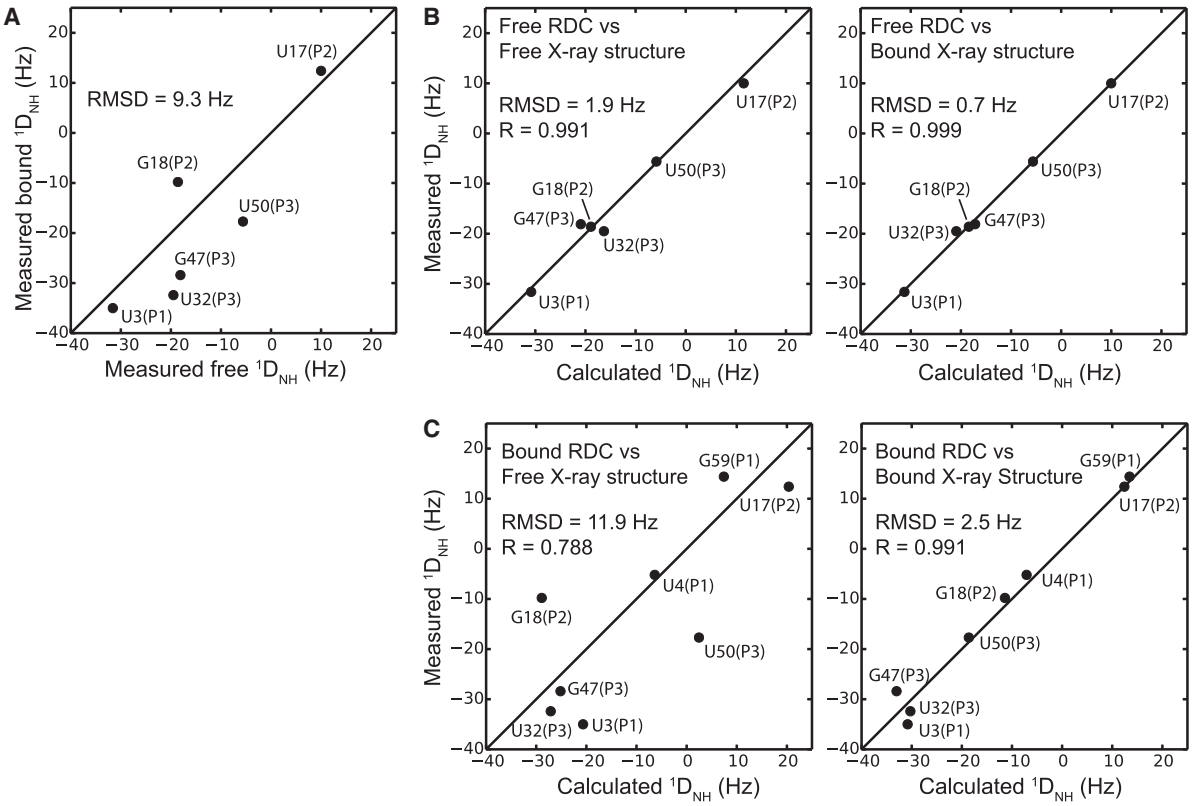

Figure 5. Correlation Plots Between Measured and Best-Fitted RDCs for E-Glutamine Riboswitch in Free and Ligand-Bound Forms

(A) Comparison of ^{1}H-^{15}N RDCs measured in the free and ligand-bound riboswitch.

(B and C) Comparison of ^{1}H-^{15}N RDCs measured in the free- (B) and bound-form (C) E-glutamine riboswitch in the presence of 5 mM Mg^{2+} with values back-calculated by best fitting the RDCs to the free- (left) and bound-form (right) crystal structures.

Residues are labeled on the RDC plots along with their stem location in parentheses.

intensities as a function of ligand concentration yields a K_d ~280–590 μM (Figure 4E), very similar to that measured for the X-ray constructs using ITC (171 μM) and for a longer construct using in-line probing assay (575 μM; Ames and Breaker, 2011). Thus, the glutamine riboswitch retains low-affinity binding under the NMR conditions.

Ligand Binding Stabilizes the P1 Helix but Destabilizes the Short Helix Below P1

The NMR data indicate that ligand binding stabilizes the P1 helix as judged based on observation of the G59 imino resonance in the P1 junctional C1-G59 base pair in the L-glutamine bound state of the E-glutamine riboswitch. This base pair immediately neighbors the long-range G23-C60 linchpin pair (Figure 4A). In line with this observation, the X-ray structure of the ligand-bound state is stabilized by stacking interactions with the linchpin G23-C60 pair. These data indicate that ligand binding stabilizes the P1 helix, including its lower portion (Figures 2B and 4A), which is in turn consistent with aMD trajectories showing that the P1 helix is more rigid in the L-glutamine-bound state (Figure 3C). The formation of P1 and its increased stabilization upon ligand binding is well documented in a subset of riboswitches by NMR and other methods and is considered a hallmark of these riboswitches (Buck et al., 2007; Lemay et al., 2006; Stoddard et al., 2008). In stark contrast to the lower portion of the P1 helix in the E-glutamine riboswitch, the addition of Mg^{2+} or both Mg^{2+} and L-glutamine resulted in the disappearance of imino resonances belonging to base pairs in the short helix below P1, including the three iminos belonging to U-3•G61 and G-4-C62 pairs (Figures 4A, 4D, and S5C).

Analysis of the Ligand-Induced Transition Using NMR RDCs

To test the validity of the X-ray structures under solution conditions, we measured NMR residual dipolar couplings (RDCs) (Tjandra and Bax, 1997; Tolman et al., 1995) for imino N-H bond vectors for the E-glutamine riboswitch in the free and ligand-bound states. RDCs are sensitive reporters of bond vector orientation and the RNA global structure. Comparison of RDCs measured in free and ligand-bound states revealed large differences consistent with a global transition in structure upon ligand binding (Figure 5A). The RDCs measured in the free state are in excellent agreement with the ligand-free X-ray structure (RMSD = 1.9 Hz; Figure 5B, left), as the experimental RDC uncertainty is ~2 Hz. In contrast, the free RDCs are not consistent with many of the structures obtained from the aMD simulation, indicating that

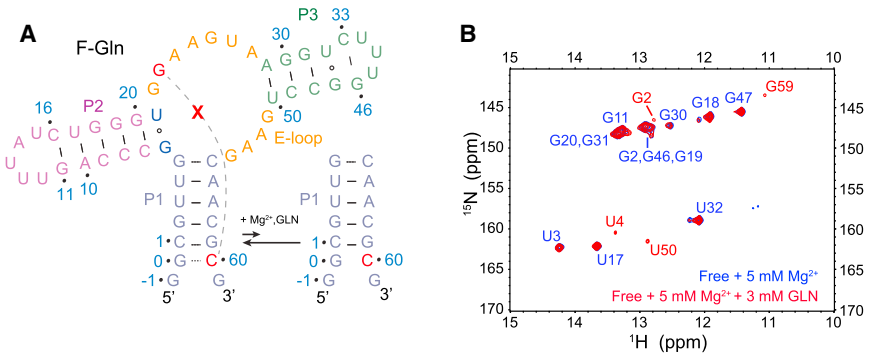

Figure 6. Increasing the Conformational Penalty to Form the Long-Range Linchpin Base Pair Results in Loss of Ligand Binding

(A) Secondary structure of a RNA construct designated F-glutamine riboswitch, which is impaired from forming a long-range linchpin by sequestering residue C60 into a G0-C60 base pair in the P1 stem.

(B) 2D NH SOFAST-HMQC spectra of F-glutamine riboswitch (100 μM) in the absence (blue) and presence (red) of 3 mM L-glutamine. All the measurements were conducted in the presence of 5 mM Mg^{2+} at 25°C. The NMR buffer was 50 mM potassium acetate at pH 6.8.

they are capable of resolving differences in the glutamine riboswitch structure (data not shown). Interestingly, the free RDCs are also highly consistent with the X-ray-determined ligand-bound structure (RMSD = 0.7 Hz; Figure 5B, right). This can either be attributed to a fortuitous coincidence that the free and bound structures are degenerate with respect to RDCs, as indicated by a condition number (Losonczi et al., 1999) as high as 18.1, or may also reflect a degree of dynamic averaging in the free state that renders the RDCs consistent with different conformations. By contrast, the RDCs measured in the ligand-bound state are in excellent agreement with the ligand-bound structure (RMSD = 2.5 Hz; Figure 5C, right) and show markedly reduced agreement with the ligand-free X-ray structure (RMSD = 11.9 Hz; Figure 5C, left), indicating that the ligand-bound glutamine riboswitch in solution indeed adopts the L-shaped conformation. These results together with the chemical shift mapping experiments (Figure 4) indicate that, despite the presence of Mg^{2+} in the crystallization buffer, the free X-ray structure captures one conformational state of the RNA that is observed in the absence of Mg^{2+}.

Mg^{2+}-Mediated Slow Exchange of E-Glutamine Riboswitch Between Free and Ligand-Bound States

Interestingly, the spectra of the glutamine riboswitch in the presence of Mg^{2+} exhibit two sets of imino resonances indicative of two species: a major state that is identical to that observed in the absence of Mg^{2+} and a minor state that is similar, but not identical, to the ligand-bound state. The 2D NH and CH HMQC spectra show that, whereas the addition of Mg^{2+} results in spectra for the minor conformer that are more similar to those of the ligand-bound state, significant differences remain (Figures S5D and S5E). Increasing the concentration of Mg^{2+} from 5 mM to 10 mM did not lead to significant increases in the intensity of these minor resonances as observed with increasing ligand concentration (data not shown), indicating that Mg^{2+} alone cannot completely stabilize a ligand-bound structure. Under these conditions, we estimate the population of the minor species to be ~15%.

It is possible that the Mg^{2+}-stabilized minor conformation observed in solution has some features in common to the bound-like conformations observed in aMD simulations in the free state (Figures 3B and 3D). The slow equilibrium between major and minor conformations in the E-glutamine riboswitch is consistent with the aMD trajectory, which indicates that the P1 helix must partially melt for the transition to occur (Figures 3B and 3D). Assuming that the Mg^{2+}-stabilized form is competent for ligand binding, we can estimate an upper limit for the ligand-bound population at <15%, yielding $K_{eq} < 0.18$ and a free energy penalty for forming the bound conformation of >1.0 kcal mol^{-1}. On the other hand, if the Mg^{2+}-bound form is not fully competent for ligand binding but rather requires additional conformational changes to achieve the ligand-competent form, the population of the bound conformation could well be <15%. Thus, conformational penalty in the glutamine riboswitch (K_{app}) can range between one to several orders of magnitude.

Increasing the Conformational Penalty toward Linchpin Formation Results in Loss of Ligand Binding

What is the origin of the conformational penalty in the glutamine riboswitch, or more specifically, why is the ligand-bound structure energetically unfavorable in the ligand-free state? A defining feature of the ligand-bound structure is a long-range linchpin G23-C60 base pair that stabilizes both the global L-shaped conformation and ligand-binding pocket. Precise formation of this single long-range base pair could be more stringent and energetically demanding as compared to tertiary motifs that are stabilized by more-extensive interactions involving more than two residues. Our aMD and coarse-grained simulations also suggest that the inter-helical angles needed to form this contact and the L-shaped conformation are disfavored by the RNA secondary structure (Figures 3 and S4). To test the importance of the linchpin interaction in ligand binding and as a potential source of a conformational penalty, we engineered a glutamine riboswitch in which formation of the linchpin is challenged by adding two guanine residues at the 5′ end (Figure 6A). These guanine residues are capable of base pairing and sequestering C60 required for forming the linchpin interaction (Figure 4A). The addition of the two guanines is expected to minimally interfere with the ligand-bound structure given their remote position relative to the binding pocket. NMR spectra of this construct were almost identical to those of the native construct in the absence of Mg^{2+}, consistent with stabilization of the free state. Remarkably, even though this engineered construct showed little to no changes in NMR chemical shifts relative to the native NMR construct, we did not observe any significant changes upon the addition of the L-glutamine ligand (Figure 6B). Thus, increasing the penalty for forming the linchpin can significantly decrease the ligand-binding affinity, highlighting the importance of the linchpin interaction in ligand binding.

DISCUSSION

The Ligand-Mediated Tuning Fork to L-shaped Conformational Transition

Our studies report one of the largest transitions in structure reported to date between free and ligand-bound forms of sensing domains in riboswitches (Figures 1 and 2). In contrast to other junctional riboswitches, the metabolite-sensing domain of the glutamine riboswitch in the free form in the crystalline state adopts a compact tuning fork architecture typically seen in the ligand-bound conformations of other riboswitches (Serganov and Patel, 2012). This was somewhat unexpected because the structure lacks the bound ligand or tertiary interactions that could hold stems P2 and P3 in approximately parallel alignment. On the other hand, stacking between three adjacent planar pairing alignments (Figures 1F–1H) contribute to stabilization of the three-way junction (Figure 1D).

On formation of the complex between L-glutamine and the glutamine riboswitch, a disordered junctional G23-G24-A25 segment becomes ordered and generates the ligand-binding pocket through a long-range linchpin Watson-Crick G23-C60 pairing alignment. Notably, whereas G54 forms limited interactions within the E-loop/P3 segment in the free form (Figure 1E), it swings toward the P1 stem in the ligand-bound form to base pair with A56 (Figure 2D). These interactions effectively remodel the three-way junction topology, and these together with the long-range linchpin G23-C60 pair help stabilize a distinct L-shaped conformation. Importantly, the bound L-glutamine is an integral part of the L-shaped three-way junction (Figure 2G), with G22, G23, and A24, that form a three-sided box that encompasses the carboxamide moiety of bound L-glutamine (Figure 2J), forming the terminal residues of the three helices that form the L-shaped scaffold (Figure 2G).

The structural transition on L-glutamine binding is supported by the in-line probing data in solution (Ames and Breaker, 2011) that revealed ligand-dependent rigidification of the three-helical junction. These in-line probing studies demonstrated cleavage reduction at positions U21, G22, G23, A24, A53, G54, and C60 (our nomenclature in Figure 1A) on complex formation (Ames and Breaker, 2011). These can be readily explained based on the available crystal structures of the sensing domain of the glutamine riboswitch in the free and L-glutamine-bound states (Figures S6A and S6B). The G22-G23-A24 segment is disordered in the free state but forms a three-sided box for encapsulation of the carboxamide side chain functionality of L-glutamine in the bound state. The pyrimidine at position 21 is located next to this disordered segment in the free state and likely forms a more-stable base pair in the ligand-bound form. Residue A53 participates in the formation of distinct elements in the two structures, suggestive of its dynamic nature in the free state. The residue G54 is unpaired in the free state, whereas it is part of a G54•(A56-U4) triple in the bound state (Figures 2B and 2D). Finally, C60 is unpaired in the free state (Figure 1C), whereas it forms the long-range linchpin G23•C60 pair in the bound state (Figure 2G).

aMD simulations (Figure 3) show a dynamic structural landscape with two energetic minima for the free-form glutamine riboswitch, one of which corresponds to the free-form RNA structure observed by X-ray crystallography and the other corresponds to a structure similar to, but not identical with, the bound-form X-ray structure. Thus, it appears likely that the free-form X-ray structure with its tuning fork architecture is one of multiple equilibrating conformations in solution in what is likely a flexible free-form RNA lacking tertiary interactions, thereby capable of transiently sampling L-shaped conformations, similar, but not identical, to those observed in the ligand-bound state.

Conformational changes in the alignment of A-form helices are a common RNA dynamic structural transition that plays essential roles in the catalytic activity of ribozymes, hierarchical assembly of ribonucleoproteins, and RNA adaptive recognition (Dethoff et al., 2012). Though ligand-induced conformational changes in riboswitches have been characterized previously by NMR, SAXS, chemical probing, and single molecule and computational studies, few studies have experimentally captured large ligand-dependent changes in riboswitch structure at atomic resolution as observed here for the glutamine riboswitch.

Binding Pocket Describes Basis for Selectivity

The crystal structures of the glutamine riboswitch showed that ligand binding stabilizes a three-helical junction, an RNA element found critical for regulation in many riboswitches (Serganov and Patel, 2012). Strikingly, the ligand-free and bound structures of the glutamine riboswitch revealed dramatically different conformations of the junction and demonstrated that the bound ligand engages dynamic and conserved residues G22, G23, and A24 in base pairing to form a three-sided box that accommodates the side chain of L-glutamine (Figures 2B and 2G) and contributes to the L-shaped alignment.

The glutamine riboswitch binds L-glutamine with very high selectivity as shown by its ability to discriminate against a range of analogs (Figures S1E and S1F; Table S1; Ames and Breaker, 2011). This can be rationalized based on the intermolecular contacts observed in the ligand-bound structure (Figures 2G, 2I, and 2J), where all heteroatoms of L-glutamine are involved in hydrogen-bonding interactions, allowing anchoring of the ends and measurement of the length and type of the side chain. An Mg^{2+} cation bound to the ligand compensates the negative charge of the carboxylate moiety and serves as an additional factor helping to discriminate between cognate and non-cognate ligands. Any modifications involving disruption of this Mg^{2+}-coordinated hydrogen-bonding network impact on the binding affinity. A similar selectivity was observed for binding of L-lysine by the lysine riboswitch, which also involved cation-mediated hydrogen bond networks that used related principles for selective recognition of L-lysine with its long hydrophobic side chain (Serganov et al., 2008).

Importantly, the glutamine riboswitch effectively discriminates against L-glutamate, which may exist in 20-fold-higher concentration than L-glutamine in bacteria (Bennett et al., 2009). This discrimination is most likely due to a hydrogen bond between the side chain CO of L-glutamine and the 4-NH_2 group of C1 (Figures 2G and 2I), which would be disrupted in the L-glutamate complex. An additional negative charge in the side chain of

L-glutamate could also play a role in electrostatics-mediated discrimination of these two ligands.

Ligand-Dependent Linchpin Stabilizes the P1 Helix and Triggers Melting of the Lower Helical Stem

A striking feature of the L-glutamine-bound state involves formation of a long-range linchpin Watson-Crick G23-C60 base pair. By contrast, residue C60 in the free state is stacked on the terminal base pair of stem P1 but is otherwise unpaired (Figure 1C), whereas G23 is part of the disordered segment (Figure 1D) in the ligand-free structure. Formation of this long-range G-C pair in the bound state is critical not just as a tertiary interaction stapling the overall architecture in an L-shaped conformation but also contributes to formation of one face of the L-glutamine-binding pocket. This dual role was unanticipated for the glutamine riboswitch, identifying this linchpin G-C pair formation as a key component of a ligand-dependent tertiary RNA switch. In particular, substitutions that sequester the guanine of the linchpin into a Watson-Crick base pair trap the free form of the RNA and strongly inhibit ligand binding (Figure 6). Further, computational simulations indicate that the long-range linchpin pair favors the L-shaped rather than the tuning fork conformation observed in the free state (data not shown). As shown in Figure 3C, the P1 helix of the L-shaped bound form is very stable under aMD simulations, and the linchpin base pair is preserved all through the simulations.

The concept of an RNA tertiary switch has been recently highlighted, whereby tethering of RNA helices in defined alignments is facilitated by long-range tertiary base pair formation (Ganser et al., 2014). In addition, long-range linchpin G-C pair stabilization of P1 has also been observed previously in the c-GMP-I (Smith et al., 2009; Kulshina et al., 2009) riboswitch. This linchpin concept has been primarily highlighted based on the recent demonstration of tRNA mimicry by a viral RNA (Colussi et al., 2014). It should be noted that, whereas a structure is available of the viral RNA held in a tRNA-like L-shaped architecture due to the linchpin interaction (Colussi et al., 2014), no structure is yet available for its counterpart in a more-open conformation on disruption of the linchpin interaction.

Open Ligand-Binding Pocket and Conformational Penalty Provide Basis for Reducing Ligand-Binding Affinity while Retaining High Selectivity

Sensing domains of riboswitches bind their ligands with a wide range of binding affinities that reflect in part the variable cellular concentrations of different metabolites. Despite the broad range, riboswitches show exquisite selectivity for their ligands, even in cases where the binding affinity is weak. The glutamine riboswitch studied here provides a striking example as one of the weakest binding-sensing domains that retains high selectivity. Our study identifies two distinct strategies that are employed by glutamine riboswitch to achieve low-affinity high-selectivity binding.

Unlike the vast majority of riboswitches, the glutamine riboswitch binds L-glutamine in an open pocket (Figure 2H). This finding is not surprising because the riboswitch is apparently tuned to high ligand concentration and an open pocket would increase the k_{off} rate and decrease the binding affinity. The ligand in two other amino-acid-sensing riboswitches, glycine and lysine riboswitches, is enveloped in the RNA structures and therefore displays over 100-fold-higher affinity (Huang et al., 2010; Serganov et al., 2008). Nevertheless, the glutamine riboswitch achieves exquisite selectivity by involving all heteroatoms of the bound ligand in direct and water-mediated hydrogen-bonding interactions in a tight pocket (Figures 2G and 2H). The combination of low affinity and high selectivity through employing an open ligand-binding pocket architecture and extensive hydrogen bonding makes the glutamine riboswitch unique, because another open pocket riboswitch, the tetrahydropholate riboswitch, has apparently evolved to sense distinct ligands that share the same core moiety (Huang et al., 2011; Trausch et al., 2011).

The NMR and MD data also indicate that, in the presence of up to 10 mM Mg^{2+}, the glutamine riboswitch exists in a slow dynamic equilibrium (relative to the NMR chemical shift timescales) between a predominant free-form and minor bound-like conformations (~15%) with Mg^{2+} stabilizing the bound-like conformation (Figures 4B–4D and S5D). These data suggest that the ligand-bound state is unfavorable in the absence of ligand. This limited sampling of the ligand-bound conformation naturally leads to an energetic conformational penalty to ligand binding. In particular, the apparent K_d will be reduced by a fraction corresponding to the population of the ligand-bound state in the absence of ligand. By applying such an energetic penalty to forming a conformation that can bind ligands with high selectivity, the binding affinity can be reduced without compromising selectivity. In contrast, reducing binding affinity by minimizing intermolecular interactions with ligand could result in loss of selectivity and non-specific binding to related ligands. In this context, it is interesting to note that the conformational penalty for forming the ligand-bound state is quite high (Figure S4C). Thus, it is possible that, in the glutamine riboswitch, the conformational penalty is encoded in part by topological constraints (Bailor et al., 2010; Mustoe et al., 2014) imposed by the three-way junction that destabilizes the L-shaped topology and also the high entropic penalty for forming a single precise long-range linchpin base pair as opposed to tertiary contacts that can involve a greater number of interaction between a larger number of residues. Further quantification of the relevant conformational dynamics across a wide range of riboswitches is ultimately required to rigorously assess the role of conformational penalties in tuning the ligand-binding affinities of riboswitches.

Biological Mechanisms Underlying *S. elongatus* Glutamine Riboswitch Function

The *glnA* motif has been found close to predicted transcription terminators and ribosomal protein sites, which may be part of expression platforms that modulate gene expression (Weinberg et al., 2010). However, the hallmark of riboswitches, namely alternative base pairing between portions of the metabolite-sensing domains and expression platforms, is not obvious in the glutamine riboswitch. Moreover, the nature of the response, gene activation or inhibition by L-glutamine, cannot be easily deduced from the sequence information. For example, the *S. elongatus* glutamine riboswitch studied here is located

immediately upstream of the gene encoding for a putative protein with unknown function (Figures S6C and S6D). The absence of a predicted transcription terminator in the vicinity of the riboswitch and close positioning of the gene and riboswitch suggest that regulation modulates initiation of translation. The gene, however, does not have a pronounced Shine-Dalgarno sequence, likely reflecting a different mechanism of translational initiation in cyanobacteria. These features of the expression platform preclude prediction of alternative conformations and the outcome of the riboswitch response.

In order to determine the mechanism of the *S. elongatus* glutamine riboswitch, we attempted to express the gene in the in vitro cell-free system prepared from *E. coli*, the Gram-negative model bacterium that is most close to cyanobacteria. However, in vitro translation did not yield a product of the expected size when the gene was expressed downstream of either a wild-type glutamine riboswitch or the 'linchpin mutant' incapable of L-glutamine binding. Deciphering the mechanism of the riboswitch will therefore require genetic manipulation in *S. elongatus*.

This work has discovered structural principles employed for the regulation of nitrogen metabolism in bacteria. These principles differ from the glutamine-dependent allosteric regulation by proteins (Leigh and Dodsworth, 2007) and highlight an important role of non-coding RNAs for micro-organisms that are essential for production of oxygen and nitrogen fixation on the planet.

EXPERIMENTAL PROCEDURES

Crystallization and Structure Determination

A riboswitch-U1A complex was prepared by mixing in-vitro-transcribed RNA and U1A protein in 100 mM potassium acetate (pH 6.8) and 5 mM $MgCl_2$, followed by gel filtration. A 0.5-mM RNA-U1A complex was mixed with 5 mM L-glutamine and incubated on ice for 1 hr. Crystals were grown by vapor diffusion after mixing the RNA-U1A or L-glutamine-RNA-U1A complexes and the reservoir solutions (0.2 M Na-formate and 21% [w/v] PEG3350 for the ligand-free structure; 0.1 M HEPES-sodium [pH 7.0], 40% [v/v] 2-methyl-2,4-pentanediol for the L-glutamine-bound structure). Crystals were cryoprotected and flash frozen in liquid nitrogen. Data were collected at 100 K. The structure was determined using molecular replacement with U1A protein and Phaser. The RNA model was built in COOT and refined in PHENIX (Table S2). Metal cation soaking was performed with 2 mM $MnCl_2$ or 20 mM CsCl for 24 hr. L-glutamine and cations were identified based on $2F_o$-F_c and F_o-F_c maps guided by the coordination geometries, coordination distances, and omit and anomalous maps. Metal-soaked structures were refined (Table S2) using the native riboswitch model. Figures were prepared with PyMol. For experimental details and other protocols, please refer to the Supplemental Experimental Procedures.

NMR and Computational Studies

NMR samples were prepared by in vitro transcription followed by denaturing PAGE or ion-exchange HPLC purification and then exchanged into NMR buffer (50 mM potassium acetate [pH 6.8]). 2D ^{15}N-edited NOESY spectra were acquired using 120-ms mixing time at 10°C. The ligand titration spectra and RDC spectra were acquired using 2D imino SOFAST-HMQC experiments. RDCs were measured by IPAP approach using imino SOFAST experiment and were fitted to crystal structures using RAMAH. All spectra were processed by NMRPipe, and spectral plots were prepared by Sparky. MD simulations were performed using GPU-accelerated Amber 12 and the ff99bsc0 force field. Prior to calculation of inter-helical angles, three-base-pair helical stretches were defined as residues 2–4 and 56–58 (P1), residues 7–9 and 18–20 (P2), and residues 30–32 and 47–49 (P3). Coarse-grained TOPRNA simulations were conducted using CHARMM program, following the procedure published elsewhere. The secondary structure of glutamine riboswitch during simulations was maintained according to the secondary structure of ligand-free conformations.

ACCESSION NUMBERS

The accession numbers for the coordinates of the X-ray structures of the glutamine riboswitch reported in this paper are: free state, RCSB: 5DDO; bound to L-glutamine, RCSB: 5DDP; Mn^{2+}-soaked in the complex, RCSB: 5DDQ; and Cs^{+}-soaked in the complex, RCSB: 5DDR.

SUPPLEMENTAL INFORMATION

Supplemental Information includes Supplemental Experimental Procedures, six figures, and two tables and can be found with this article online at http://dx.doi.org/10.1016/j.celrep.2015.10.062.

AUTHOR CONTRIBUTIONS

A.R. designed the sensing domain constructs of the glutamine riboswitch, crystallized the riboswitches, determined the structures, and performed ITC-binding experiments under the supervision of D.J.P. Y.X. performed the NMR and MD simulations under the supervision of H.M.A.-H. A.P. performed RNA probing and functional experiments (data not shown) under the supervision of A.S. The manuscript was written by A.S., H.M.A.-H., and D.J.P. All authors discussed the results and commented on the manuscript.

ACKNOWLEDGMENTS

We thank the personnel of NE-CAT beamlines at the Advanced Photon Source, Argonne National Laboratory, funded by the US Department of Energy for assistance with data collection. We thank Satoko Ishibe-Murakami (Memorial Sloan-Kettering Cancer Center) for assistance with denaturing polyacrylamide gel preparation. D.J.P. was supported by funds from the NIH (1 U19 CA179564). H.M.A.-H. was supported by funds from the NIH (P01 GM0066275). A.S. was supported by start-up funds from New York University and NIH grant R01 GM112940. A.P. was supported by the NIH 5T32GM088118-05. D.J.P acknowledges support by the Memorial Sloan-Kettering Cancer Center Support Grant/Core Grant (P30 CA008748).

Received: March 26, 2015
Revised: August 17, 2015
Accepted: October 20, 2015
Published: November 19, 2015

REFERENCES

Ames, T.D., and Breaker, R.R. (2011). Bacterial aptamers that selectively bind glutamine. RNA Biol. *8*, 82–89.

Auffinger, P. (2012). Ions in molecular dynamics simulations of RNA systems. In RNA 3D Structure Analysis and Prediction, N. Leontis and E. Westhof, eds. (Springer Berlin Heidelberg), pp. 299–318.

Bailor, M.H., Sun, X., and Al-Hashimi, H.M. (2010). Topology links RNA secondary structure with global conformation, dynamics, and adaptation. Science *327*, 202–206.

Bailor, M.H., Mustoe, A.M., Brooks, C.L., 3rd, and Al-Hashimi, H.M. (2011). 3D maps of RNA interhelical junctions. Nat. Protoc. *6*, 1536–1545.

Bennett, B.D., Kimball, E.H., Gao, M., Osterhout, R., Van Dien, S.J., and Rabinowitz, J.D. (2009). Absolute metabolite concentrations and implied enzyme active site occupancy in Escherichia coli. Nat. Chem. Biol. *5*, 593–599.

Bothe, J.R., Nikolova, E.N., Eichhorn, C.D., Chugh, J., Hansen, A.L., and Al-Hashimi, H.M. (2011). Characterizing RNA dynamics at atomic resolution using solution-state NMR spectroscopy. Nat. Methods *8*, 919–931.

Breaker, R.R. (2011). Prospects for riboswitch discovery and analysis. Mol. Cell *43*, 867–879.

Buck, J., Fürtig, B., Noeske, J., Wöhnert, J., and Schwalbe, H. (2007). Time-resolved NMR methods resolving ligand-induced RNA folding at atomic resolution. Proc. Natl. Acad. Sci. USA *104*, 15699–15704.

Butler, E.B., Xiong, Y., Wang, J., and Strobel, S.A. (2011). Structural basis of cooperative ligand binding by the glycine riboswitch. Chem. Biol. *18*, 293–298.

Chen, B., Zuo, X., Wang, Y.X., and Dayie, T.K. (2012). Multiple conformations of SAM-II riboswitch detected with SAXS and NMR spectroscopy. Nucleic Acids Res. *40*, 3117–3130.

Colussi, T.M., Costantino, D.A., Hammond, J.A., Ruehle, G.M., Nix, J.C., and Kieft, J.S. (2014). The structural basis of transfer RNA mimicry and conformational plasticity by a viral RNA. Nature *511*, 366–369.

Correll, C.C., Freeborn, B., Moore, P.B., and Steitz, T.A. (1997). Metals, motifs, and recognition in the crystal structure of a 5S rRNA domain. Cell *91*, 705–712.

Dethoff, E.A., Chugh, J., Mustoe, A.M., and Al-Hashimi, H.M. (2012). Functional complexity and regulation through RNA dynamics. Nature *482*, 322–330.

Ganser, L.R., Mustoe, A.M., and Al-Hashimi, H.M. (2014). An RNA tertiary switch by modifying how helices are tethered. Genome Biol. *15*, 425.

Garst, A.D., Héroux, A., Rambo, R.P., and Batey, R.T. (2008). Crystal structure of the lysine riboswitch regulatory mRNA element. J. Biol. Chem. *283*, 22347–22351.

Green, N.J., Grundy, F.J., and Henkin, T.M. (2010). The T box mechanism: tRNA as a regulatory molecule. FEBS Lett. *584*, 318–324.

Grundy, F.J., Lehman, S.C., and Henkin, T.M. (2003). The L box regulon: lysine sensing by leader RNAs of bacterial lysine biosynthesis genes. Proc. Natl. Acad. Sci. USA *100*, 12057–12062.

Hamelberg, D., Mongan, J., and McCammon, J.A. (2004). Accelerated molecular dynamics: a promising and efficient simulation method for biomolecules. J. Chem. Phys. *120*, 11919–11929.

Huang, L., Serganov, A., and Patel, D.J. (2010). Structural insights into ligand recognition by a sensing domain of the cooperative glycine riboswitch. Mol. Cell *40*, 774–786.

Huang, L., Ishibe-Murakami, S., Patel, D.J., and Serganov, A. (2011). Long-range pseudoknot interactions dictate the regulatory response in the tetrahydrofolate riboswitch. Proc. Natl. Acad. Sci. USA *108*, 14801–14806.

Jenkins, J.L., Krucinska, J., McCarty, R.M., Bandarian, V., and Wedekind, J.E. (2011). Comparison of a preQ$_1$ riboswitch aptamer in metabolite-bound and free states with implications for gene regulation. J. Biol. Chem. *286*, 24626–24637.

Klein, D.J., Edwards, T.E., and Ferré-D'Amaré, A.R. (2009). Cocrystal structure of a class I preQ$_1$ riboswitch reveals a pseudoknot recognizing an essential hypermodified nucleobase. Nat. Struct. Mol. Biol. *16*, 343–344.

Kulshina, N., Baird, N.J., and Ferré-D'Amaré, A.R. (2009). Recognition of the bacterial second messenger cyclic diguanylate by its cognate riboswitch. Nat. Struct. Mol. Biol. *16*, 1212–1217.

Leigh, J.A., and Dodsworth, J.A. (2007). Nitrogen regulation in bacteria and archaea. Annu. Rev. Microbiol. *61*, 349–377.

Lemay, J.F., Penedo, J.C., Tremblay, R., Lilley, D.M., and Lafontaine, D.A. (2006). Folding of the adenine riboswitch. Chem. Biol. *13*, 857–868.

Losonczi, J.A., Andrec, M., Fischer, M.W., and Prestegard, J.H. (1999). Order matrix analysis of residual dipolar couplings using singular value decomposition. J. Magn. Reson. *138*, 334–342.

Mandal, M., Lee, M., Barrick, J.E., Weinberg, Z., Emilsson, G.M., Ruzzo, W.L., and Breaker, R.R. (2004). A glycine-dependent riboswitch that uses cooperative binding to control gene expression. Science *306*, 275–279.

Mironov, A.S., Gusarov, I., Rafikov, R., Lopez, L.E., Shatalin, K., Kreneva, R.A., Perumov, D.A., and Nudler, E. (2002). Sensing small molecules by nascent RNA: a mechanism to control transcription in bacteria. Cell *111*, 747–756.

Montange, R.K., and Batey, R.T. (2006). Structure of the *S*-adenosylmethionine riboswitch regulatory mRNA element. Nature *441*, 1172–1175.

Mustoe, A.M., Brooks, C.L., 3rd, and Al-Hashimi, H.M. (2014). Topological constraints are major determinants of tRNA tertiary structure and dynamics and provide basis for tertiary folding cooperativity. Nucleic Acids Res. *42*, 11792–11804.

Nahvi, A., Sudarsan, N., Ebert, M.S., Zou, X., Brown, K.L., and Breaker, R.R. (2002). Genetic control by a metabolite binding mRNA. Chem. Biol. *9*, 1043.

Oubridge, C., Ito, N., Teo, C.H., Fearnley, I., and Nagai, K. (1995). Crystallisation of RNA-protein complexes. II. The application of protein engineering for crystallisation of the U1A protein-RNA complex. J. Mol. Biol. *249*, 409–423.

Serganov, A., and Patel, D.J. (2012). Metabolite recognition principles and molecular mechanisms underlying riboswitch function. Annu. Rev. Biophys. *41*, 343–370.

Serganov, A., and Nudler, E. (2013). A decade of riboswitches. Cell *152*, 17–24.

Serganov, A., Yuan, Y.R., Pikovskaya, O., Polonskaia, A., Malinina, L., Phan, A.T., Hobartner, C., Micura, R., Breaker, R.R., and Patel, D.J. (2004). Structural basis for discriminative regulation of gene expression by adenine- and guanine-sensing mRNAs. Chem. Biol. *11*, 1729–1741.

Serganov, A., Huang, L., and Patel, D.J. (2008). Structural insights into amino acid binding and gene control by a lysine riboswitch. Nature *455*, 1263–1267.

Smith, K.D., Lipchock, S.V., Ames, T.D., Wang, J., Breaker, R.R., and Strobel, S.A. (2009). Structural basis of ligand binding by a c-di-GMP riboswitch. Nat. Struct. Mol. Biol. *16*, 1218–1223.

Stoddard, C.D., Gilbert, S.D., and Batey, R.T. (2008). Ligand-dependent folding of the three-way junction in the purine riboswitch. RNA *14*, 675–684.

Stoddard, C.D., Montange, R.K., Hennelly, S.P., Rambo, R.P., Sanbonmatsu, K.Y., and Batey, R.T. (2010). Free state conformational sampling of the SAM-I riboswitch aptamer domain. Structure *18*, 787–797.

Sudarsan, N., Wickiser, J.K., Nakamura, S., Ebert, M.S., and Breaker, R.R. (2003). An mRNA structure in bacteria that controls gene expression by binding lysine. Genes Dev. *17*, 2688–2697.

Tjandra, N., and Bax, A. (1997). Direct measurement of distances and angles in biomolecules by NMR in a dilute liquid crystalline medium. Science *278*, 1111–1114.

Tolman, J.R., Flanagan, J.M., Kennedy, M.A., and Prestegard, J.H. (1995). Nuclear magnetic dipole interactions in field-oriented proteins: information for structure determination in solution. Proc. Natl. Acad. Sci. USA *92*, 9279–9283.

Trausch, J.J., Ceres, P., Reyes, F.E., and Batey, R.T. (2011). The structure of a tetrahydrofolate-sensing riboswitch reveals two ligand binding sites in a single aptamer. Structure *19*, 1413–1423.

Weinberg, Z., Wang, J.X., Bogue, J., Yang, J., Corbino, K., Moy, R.H., and Breaker, R.R. (2010). Comparative genomics reveals 104 candidate structured RNAs from bacteria, archaea, and their metagenomes. Genome Biol. *11*, R31.

Wickiser, J.K., Winkler, W.C., Breaker, R.R., and Crothers, D.M. (2005). The speed of RNA transcription and metabolite binding kinetics operate an FMN riboswitch. Mol. Cell *18*, 49–60.

Winkler, W., Nahvi, A., and Breaker, R.R. (2002). Thiamine derivatives bind messenger RNAs directly to regulate bacterial gene expression. Nature *419*, 952–956.

Zhang, J., Jones, C.P., and Ferré-D'Amaré, A.R. (2014). Global analysis of riboswitches by small-angle X-ray scattering and calorimetry. Biochim. Biophys. Acta *1839*, 1020–1029.